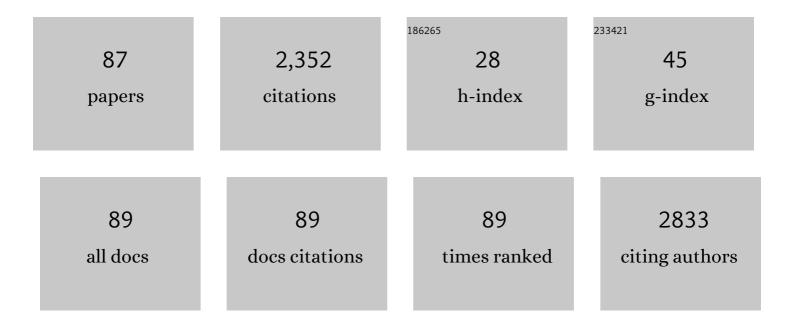
## Cuizhen Wang

List of Publications by Year in descending order

Source: https://exaly.com/author-pdf/2541461/publications.pdf Version: 2024-02-01



#	Article	IF	CITATIONS
1	Unmanned aerial remote sensing of coastal vegetation: A review. Annals of GIS, 2022, 28, 385-399.	3.1	13
2	Deep Learning of High-Resolution Aerial Imagery for Coastal Marsh Change Detection: A Comparative Study. ISPRS International Journal of Geo-Information, 2022, 11, 100.	2.9	10
3	Off-peak NDVI correction to reconstruct Landsat time series for post-fire recovery in high-latitude forests. International Journal of Applied Earth Observation and Geoinformation, 2022, 107, 102704.	2.8	3
4	Spatiotemporal assessment of potential drivers of salt marsh dieback in the North Inlet-Winyah Bay estuary, South Carolina (1990–2019). Journal of Environmental Management, 2022, 313, 114907.	7.8	2
5	Assessing 40 years of spatial dynamics and patterns in megacities along the Belt and Road region using satellite imagery. International Journal of Digital Earth, 2021, 14, 71-87.	3.9	15
6	A 100 m population grid in the CONUS by disaggregating census data with open-source Microsoft building footprints. Big Earth Data, 2021, 5, 112-133.	4.4	32
7	High-latitude snowfall as a sensitive indicator of climate warming: A case study of Heilongjiang Province, China. Ecological Indicators, 2021, 122, 107249.	6.3	7
8	sUAS for 3D Tree Surveying: Comparative Experiments on a Closed-Canopy Earthen Dam. Forests, 2021, 12, 659.	2.1	8
9	RGB Indices and Canopy Height Modelling for Mapping Tidal Marsh Biomass from a Small Unmanned Aerial System. Remote Sensing, 2021, 13, 3406.	4.0	8
10	Mapping salt marsh along coastal South Carolina using U-Net. ISPRS Journal of Photogrammetry and Remote Sensing, 2021, 179, 121-132.	11.1	30
11	Gap-Filling of 8-Day Terra MODIS Daytime Land Surface Temperature in High-Latitude Cold Region with Generalized Additive Models (GAM). Remote Sensing, 2021, 13, 3667.	4.0	6
12	At-Sensor Radiometric Correction of a Multispectral Camera (RedEdge) for sUAS Vegetation Mapping. Sensors, 2021, 21, 8224.	3.8	5
13	Identifying disaster related social media for rapid response: a visual-textual fused CNN architecture. International Journal of Digital Earth, 2020, 13, 1017-1039.	3.9	23
14	Detecting new building construction in urban areas based on images of small unmanned aerial system. Papers in Applied Geography, 2020, 6, 56-71.	1.4	5
15	Using sUAS-Derived Point Cloud to Supplement LiDAR Returns for Improved Canopy Height Model on Earthen Dams. Papers in Applied Geography, 2020, 6, 436-448.	1.4	2
16	Choosing an appropriate training set size when using existing data to train neural networks for land cover segmentation. Annals of GIS, 2020, 26, 329-342.	3.1	12
17	Identifying marsh dieback events from Landsat image series (1998–2018) with an Autoencoder in the NIWB estuary, South Carolina. International Journal of Digital Earth, 2020, 13, 1467-1483.	3.9	10
18	Remote Sensing Derived Indices for Tracking Urban Land Surface Change in Case of Earthquake Recovery. Remote Sensing, 2020, 12, 895.	4.0	12

#	Article	IF	CITATIONS
19	Applying a rule-based object-based image analysis approach for nearshore bar identification and characterization. Journal of Applied Remote Sensing, 2020, 14, .	1.3	2
20	Prototyping a Social Media Flooding Photo Screening System Based on Deep Learning. ISPRS International Journal of Geo-Information, 2020, 9, 104.	2.9	33
21	Estimating Aboveground Biomass and Its Spatial Distribution in Coastal Wetlands Utilizing Planet Multispectral Imagery. Remote Sensing, 2019, 11, 2020.	4.0	27
22	Characterizing the changing environment of cropland in the Songnen Plain, Northeast China, from 1990 to 2015. Journal of Chinese Geography, 2019, 29, 658-674.	3.9	10
23	Comparing Sentinel-2 MSI and Landsat 8 OLI in soil salinity detection: a case study of agricultural lands in coastal North Carolina. International Journal of Remote Sensing, 2019, 40, 6134-6153.	2.9	65
24	Monitoring 40-Year Lake Area Changes of the Qaidam Basin, Tibetan Plateau, Using Landsat Time Series. Remote Sensing, 2019, 11, 343.	4.0	27
25	Human Settlement Dynamics in Hurricane-Prone Zones of Conterminous U.S: A View from Nighttime Remote Sensing. , 2019, , .		0
26	Extracting Urban Impervious Surface from WorldView-2 and Airborne LiDAR Data Using 3D Convolutional Neural Networks. Journal of the Indian Society of Remote Sensing, 2019, 47, 401-412.	2.4	26
27	A visual–textual fused approach to automated tagging of flood-related tweets during a flood event. International Journal of Digital Earth, 2019, 12, 1248-1264.	3.9	30
28	Image Processing and Analysis Methods. , 2019, , 631-868.		0
29	Carbon Flux Phenology from the Sky: Evaluation for Maize and Soybean. Journal of Atmospheric and Oceanic Technology, 2018, 35, 877-892.	1.3	3
30	A near real-time flood-mapping approach by integrating social media and post-event satellite imagery. Annals of GIS, 2018, 24, 113-123.	3.1	53
31	A novel approach to leveraging social media for rapid flood mapping: a case study of the 2015 South Carolina floods. Cartography and Geographic Information Science, 2018, 45, 97-110.	3.0	148
32	Mapping Soil Alkalinity and Salinity in Northern Songnen Plain, China with the HJ-1 Hyperspectral Imager Data and Partial Least Squares Regression. Sensors, 2018, 18, 3855.	3.8	28
33	Mapping Inter-Annual Land Cover Variations Automatically Based on a Novel Sample Transfer Method. Remote Sensing, 2018, 10, 1457.	4.0	6
34	Spatial Assessment of Water Quality with Urbanization in 2007–2015, Shanghai, China. Remote Sensing, 2018, 10, 1024.	4.0	13
35	Geospatial Assessment of Wetness Dynamics in the October 2015 SC Flood with Remote Sensing and Social Media. Southeastern Geographer, 2018, 58, 164-180.	0.2	6
36	Impacts of Agricultural Expansion (1910s–2010s) on the Water Cycle in the Songneng Plain, Northeast China. Remote Sensing, 2018, 10, 1108.	4.0	13

#	Article	IF	CITATIONS
37	Reconstructing Flood Inundation Probability by Enhancing Near Real-Time Imagery With Real-Time Gauges and Tweets. IEEE Transactions on Geoscience and Remote Sensing, 2018, 56, 4691-4701.	6.3	31
38	Geospatial assessment of bioenergy land use and its impacts on soil erosion in the U.S. Midwest. Journal of Environmental Management, 2017, 190, 188-196.	7.8	17
39	Energy crop mapping with enhanced TM/MODIS time series in the BCAP agricultural lands. ISPRS Journal of Photogrammetry and Remote Sensing, 2017, 124, 133-143.	11.1	26
40	Satellite monitoring of boreal forest phenology and its climatic responses in Eurasia. International Journal of Remote Sensing, 2017, 38, 5446-5463.	2.9	22
41	Estimation of rice grain yield from dual-polarization Radarsat-2 SAR data by integrating a rice canopy scattering model and a genetic algorithm. International Journal of Applied Earth Observation and Geoinformation, 2017, 57, 75-85.	2.8	27
42	Assessing Re-Composition of Xing'an Larch in Boreal Forests after the 1987 Fire, Northeast China. Remote Sensing, 2017, 9, 504.	4.0	9
43	Mapping Typical Urban LULC from Landsat Imagery without Training Samples or Self-Defined Parameters. Remote Sensing, 2017, 9, 700.	4.0	18
44	Mapping Urban Bare Land Automatically from Landsat Imagery with a Simple Index. Remote Sensing, 2017, 9, 249.	4.0	66
45	Environmental Influences on Forest Fire Regime in the Greater Hinggan Mountains, Northeast China. Forests, 2017, 8, 372.	2.1	20
46	A Modified Normalized Difference Impervious Surface Index (MNDISI) for Automatic Urban Mapping from Landsat Imagery. Remote Sensing, 2017, 9, 942.	4.0	64
47	Mapping salt marsh dieback and condition in South Carolina's North Inlet-Winyah Bay National Estuarine Research Reserve using remote sensing. AIMS Environmental Science, 2017, 4, 677-689.	1.4	12
48	Remote Sensing of Soil Alkalinity and Salinity in the Wuyu'er-Shuangyang River Basin, Northeast China. Remote Sensing, 2016, 8, 163.	4.0	52
49	A remote sensing perspective of alpine grasslands on the Tibetan Plateau: Better or worse under "Tibet Warming�. Remote Sensing Applications: Society and Environment, 2016, 3, 36-44.	1.5	14
50	Spatial assessment of sewage discharge with urbanization in 2004–2014, Beijing, China. AIMS Environmental Science, 2016, 3, 842-857.	1.4	3
51	MODIS-Derived Spatiotemporal Changes of Major Lake Surface Areas in Arid Xinjiang, China, 2000–2014. Water (Switzerland), 2015, 7, 5731-5751.	2.7	22
52	MODIS-Based Fractional Crop Mapping in the U.S. Midwest with Spatially Constrained Phenological Mixture Analysis. Remote Sensing, 2015, 7, 512-529.	4.0	15
53	Evaluation of Three MODIS-Derived Vegetation Index Time Series for Dryland Vegetation Dynamics Monitoring. Remote Sensing, 2015, 7, 7597-7614.	4.0	74
54	Object-Based Crop Classification with Landsat-MODIS Enhanced Time-Series Data. Remote Sensing, 2015, 7, 16091-16107.	4.0	94

#	Article	IF	CITATIONS
55	Improved POLSAR Image Classification by the Use of Multi-Feature Combination. Remote Sensing, 2015, 7, 4157-4177.	4.0	20
56	Snow effects on alpine vegetation in the Qinghai-Tibetan Plateau. International Journal of Digital Earth, 2015, 8, 58-75.	3.9	42
57	Improved alpine grassland mapping in the Tibetan Plateau with MODIS time series: a phenology perspective. International Journal of Digital Earth, 2015, 8, 133-152.	3.9	8
58	Assessing phenological change and climatic control of alpine grasslands in the Tibetan Plateau with MODIS time series. International Journal of Biometeorology, 2015, 59, 11-23.	3.0	64
59	Potential of X-Band Images from High-Resolution Satellite SAR Sensors to Assess Growth and Yield in Paddy Rice. Remote Sensing, 2014, 6, 5995-6019.	4.0	34
60	Vegetation phenology monitoring with SeaWinds scatterometer in eastern Asia. , 2014, , .		0
61	Improved Building Extraction With Integrated Decomposition of Time-Frequency and Entropy-Alpha Using Polarimetric SAR Data. IEEE Journal of Selected Topics in Applied Earth Observations and Remote Sensing, 2014, 7, 4058-4068.	4.9	21
62	The long-term trends (1982–2006) in vegetation greenness of the alpine ecosystem in the Qinghai-Tibetan Plateau. Environmental Earth Sciences, 2014, 72, 1827-1841.	2.7	49
63	Detecting winter wheat phenology with SPOT-VEGETATION data in the North China Plain. Geocarto International, 2014, 29, 244-255.	3.5	49
64	Capability of C-band backscattering coefficients from high-resolution satellite SAR sensors to assess biophysical variables in paddy rice. Remote Sensing of Environment, 2014, 140, 257-266.	11.0	140
65	Spatial patterns of land surface phenology relative to monthly climate variations: US Great Plains. GIScience and Remote Sensing, 2014, 51, 30-50.	5.9	18
66	Retrieving canopy height and density of paddy rice from Radarsat-2 images with a canopy scattering model. International Journal of Applied Earth Observation and Geoinformation, 2014, 28, 170-180.	2.8	38
67	Synergistic Use of Optical and PolSAR Imagery for Urban Impervious Surface Estimation. Photogrammetric Engineering and Remote Sensing, 2014, 80, 91-102.	0.6	28
68	Assessing bioenergy-driven agricultural land use change and biomass quantities in the U.S. Midwest with MODIS time series. Journal of Applied Remote Sensing, 2014, 8, 085198.	1.3	14
69	Monitoring bidecadal development of urban agglomeration with remote sensing images in the Jing-Jin-Tang area, China. Journal of Applied Remote Sensing, 2014, 8, 084592.	1.3	8
70	Phenology-assisted classification of C3 and C4 grasses in the U.S. Great Plains and their climate dependency with MODIS time series. Remote Sensing of Environment, 2013, 138, 90-101.	11.0	50
71	Vegetation greenness trend (2000 to 2009) and the climate controls in the Qinghai-Tibetan Plateau. Journal of Applied Remote Sensing, 2013, 7, 073572.	1.3	68
72	Assessment of the SeaWinds scatterometer for vegetation phenology monitoring across China. International Journal of Remote Sensing, 2013, 34, 5551-5568.	2.9	9

#	Article	IF	CITATIONS
73	Spatiotemporal variations of satellite-derived phenology in the Tibetan Plateau. , 2012, , .		1
74	Detecting Cutleaf Teasel ( <i>Dipsacus laciniatus</i> ) along a Missouri Highway with Hyperspectral Imagery. Invasive Plant Science and Management, 2012, 5, 155-163.	1.1	9
75	Support vector machine approach to identifying buildings using multi-temporal ALOS/PALSAR data. International Journal of Remote Sensing, 2011, 32, 7163-7177.	2.9	4
76	Phenology-Based Assessment of Perennial Energy Crops in North American Tallgrass Prairie. Annals of the American Association of Geographers, 2011, 101, 742-751.	3.0	30
77	Identifying paddy fields with dual-polarization ALOS/PALSAR data. Canadian Journal of Remote Sensing, 2011, 37, 103-111.	2.4	13
78	Trajectory-based warm season grassland mapping in Missouri prairies with multi-temporal ASTER imagery. Remote Sensing of Environment, 2010, 114, 531-539.	11.0	25
79	Mapping paddy rice with multitemporal ALOS/PALSAR imagery in southeast China. International Journal of Remote Sensing, 2009, 30, 6301-6315.	2.9	111
80	Characterizing L-Band Scattering of Paddy Rice in Southeast China With Radiative Transfer Model and Multitemporal ALOS/PALSAR Imagery. IEEE Transactions on Geoscience and Remote Sensing, 2009, 47, 988-998.	6.3	75
81	A digital earth prototype system: DEPS/CAS. International Journal of Digital Earth, 2009, 2, 3-15.	3.9	43
82	Detecting Invasive Sericea Lespedeza (Lespedeza cuneata) in Mid-Missouri Pastureland Using Hyperspectral Imagery. Environmental Management, 2008, 41, 853-862.	2.7	23
83	Mapping Paddy Rice Biomass Using ALOS/PALSAR Imagery. , 2008, , .		0
84	Biophysical estimation in tropical forests using JERSâ€1 VNIR imagery. I: Leaf area index. International Journal of Remote Sensing, 2008, 29, 6811-6826.	2.9	6
85	Biophysical estimation in tropical forests using JERSâ€∎ SAR and VNIR imagery. II. Aboveground woody biomass. International Journal of Remote Sensing, 2008, 29, 6827-6849.	2.9	48
86	Biophysical Estimation of Paddy Rice with Canopy Scattering Model and ALOS/PALSAR Imagery in Southeast China. , 2008, , .		2
87	Analysis of temporal radar backscatter of rice: A comparison of SAR observations with modeling results. Canadian Journal of Remote Sensing, 2002, 28, 128-138.	2.4	23